Journal of Magnetic Resonance **145,** 291–301 (2000)
doi:10.1006/jmre.2000.2093, available online at http://www.idealibrary.com on IDEAL®

Evidence of Red Cell Alignment in the Magnetic Field of an NMR Spectrometer Based on the Diffusion Tensor of Water

Philip W. Kuchel,* Christopher J. Durrant,† Bogdan E. Chapman,* Penelope S. Jarrett,* and David G. Regan*

**Department of Biochemistry, and †School of Mathematics and Statistics, University of Sydney, New South Wales 2006, Australia*

Received December 3, 1999; revised March 6, 2000

The alignment of human erythrocytes in aqueous suspensions in the magnetic field $\mathbf{B}_0$ (called the *z*-direction) of an NMR spectrometer was shown by calculating the diffusion tensor for water in the sample. The diffusion was measured using a pulsed-field-gradient spin-echo NMR method. The extent of diffusion anisotropy for water was exemplified by the values of the apparent diffusion coefficients with erythrocytes of normal shape and volume: for a typical experiment the values for the *x*-, *y*-, and *z*-directions were $(6.88 \pm 0.17) \times 10^{-10}$, $(7.07 \pm 0.17) \times 10^{-10}$, and $(10.20 \pm 0.17) \times 10^{-10}$ m^2 s^{-1}, respectively. Cells in hypo- and hyperosmotic media were also studied and they too showed the anisotropy of the apparent diffusion coefficients but the extents were different. A new method of data analysis was developed using the Standard Add-On Packages in a *Mathematica* program. The experimental findings support evidence of erythrocyte alignment that was previously obtained with a high-field-gradient *q*-space method.

Key Words: **cell alignment; PGSE NMR; water diffusion; multivariate analysis; erythrocytes; magnetic field effect on cells.**

INTRODUCTION

NMR-based evidence that biconcave-shape human erythrocytes in suspension in an aqueous medium become aligned in the magnetic field $\mathbf{B}_0$ of an NMR spectrometer is surprisingly recent. It was provided by the observation of coherence peaks in *q*-space plots obtained from erythrocytes that were studied with pulsed-field-gradient spin-echo (PGSE) NMR spectroscopy (*1*). A simple mathematical relationship exists between the position of the minima in these *q*-space plots and the average main diameter of the cells that are aligned with their disc-like faces parallel to $\mathbf{B}_0$ (*2, 3*). The experiments require access to a sample probe that generates very large magnetic field gradients, of the order of 2 to 10 T m^{-1}, and these are not common. Also, the probes usually generate a gradient in only one coordinate direction, parallel to $\mathbf{B}_0$ (i.e., a *z*-only gradient probe). On the other hand, there is much current interest in diffusion tensor analysis for characterizing the orientation of microstructures in tissues *in vivo* during magnetic resonance imaging (MRI) (*4–9*). The gradient coils for whole body imaging, and their high-resolution NMR counterparts, generate relatively weak magnetic field gradients that are of the order of 5 to 50 mT m^{-1} (e.g., *6, 8, 10*).

Thus, we set out to determine whether diffusion tensor analysis would provide corroborating evidence of erythrocyte alignment in $\mathbf{B}_0$ using the alternative technology and data processing procedures of diffusion tensor analysis (*4, 5*).

Because biological tissues are ordered on the microscopic scale the diffusion of solutes and water in them is often seen to be anisotropic (*4, 5*). However, this is not an obvious state for cells in a suspension except if they are not spherically symmetrical and experience an aligning force; this situation pertains to the human erythrocyte.

Tissue anisotropy can be expressed in terms of a 3×3 matrix of diffusion coefficients, or a rank two tensor (*4*). The elements of this tensor determined in contemporary MRI investigations are interpreted in terms of the locally ordered orientation of (semi-)impermeable barriers. Thus the location of axon-fiber tracts can be determined in MRI scans of the brain (*9*).

Previous explanations of the method for determining the values of the elements of the diffusion tensor (*4–10*) seemed to us to be unduly complicated; this is especially true now that several well-known computer software packages contain the requisite multivariate regression algorithms and matrix-diagonalization procedures as standard routines. In *Mathematica* (*11*) the functions Regress, NonLinearRegress, and SingularValues perform the essential roles, thus making the implementation of diffusion tensor analysis facile.

Before presenting the experimental results that were analyzed using a program written in *Mathematica,* it is pertinent to give some background theory so that the alternative analytical approach can be set in its correct context.

THEORY

The PGSE Experiment

Consider a PGSE experiment conducted on a sample which is isotropic and in which the diffusion is unbounded. Take a coordinate system with the *z*-axis in the direction of the polarizing field and let $\mathbf{k}$ be the unit vector in this direction so that

1090-7807/00 $35.00

$B_0 = B_0\,\mathbf{k}$. In this experiment the signal characteristics are determined by the gradients imposed on the component of the magnetic field in the direction of $\mathbf{B}_0$. Let this component be $B(x, y, z, t)$. In its simplest implementation the field-gradient pulses are along only one axis, usually the z-axis so that $B(x, y, z, t) = B(z, t)$. The pulses produce a uniform field-gradient $dB/dz = g_z(t)$ so that $B(z, t) = B_0 + g_z(t)z$. The field-gradient pulse is modulated in time, thus it can be written quite generally as $g_z(t) = g_{z,m}p(t)$, where $g_{z,m}$ is the maximum value of the field gradient achieved during the pulse and $p(t)$ is a profile factor. For a rectangular pulse, $p(t) = 1$ during the pulse $0 \le t \le \delta$, and $p(t) = 0$ outside the time of the pulse.

The ratio of the NMR signal intensity obtained with a nonzero field-gradient, relative to that obtained when it is zero, is referred to as the attenuation. The natural logarithm of the attenuation is denoted by R (*4, 12*):

$$R = \ln\left(\frac{S[g]}{S[0]}\right) = -\gamma^2 P^2 g_{z,m}^2 D, \qquad [1]$$

where γ is the magnetogyric ratio of the detected nucleus, D is the diffusion coefficient of the spin-bearing molecules, and P^2 is a function of the shape profile of the pulses:

$$P^2 = \int_0^{TE/2}\left[\int_0^t p(t')dt'\right]^2 dt + \int_{TE/2}^{TE}\left[\int_0^t p(t')dt' - 2\int_0^{TE/2} p(t')dt'\right]^2 dt, \qquad [2]$$

where TE is the spin-echo time. For rectangular pulses, each of duration δ and separated from each other by an interval of Δ, $P^2 = \delta^2(\Delta - \delta/3)$ [*12*].

The value of D is the negative of the slope of the line that is regressed onto the data pairs (b_i^2, R_i), $i = 1, \ldots, N$, where $b_i^2 = \gamma^2\delta^2(\Delta - \delta/3)g_{z,m,i}^2$ and is referred to as the Stejskal–Tanner parameter (*12*), and N is the number of different $g_{z,m,i}$ values used in the experiment, with a fixed pulse shape.

Requirement for a Diffusion Tensor

When the sample has barriers such as cell membranes, which are semi-permeable to the diffusant, the apparent (measured) diffusion coefficient is less than that for free diffusion (e.g., *1–5*). The value of R (Eq. [1]) varies inversely as a function of the separation distance between the restricting boundaries. Thus for a sample such as a section of brain tissue, where there are bundles of axonal fibers, the apparent diffusion coefficient of water depends on the orientation of the fibers relative to the direction of the magnetic field-gradient pulses. The dependence of D on direction requires D to be treated not as a single scalar quantity but as an array of values that will describe the diffusion behavior in all directions. The mathematical form of D is a second-rank tensor $\mathbf{D}$ with nine elements as is defined here (but it is explained further below):

$$\mathbf{D} = \begin{bmatrix} D_{11} & D_{12} & D_{13} \\ D_{21} & D_{22} & D_{23} \\ D_{31} & D_{32} & D_{33} \end{bmatrix}. \qquad [3]$$

Modern triple-axis NMR gradient probes enable the application of any combination of field-gradient pulses along three Cartesian axes. Thus the directions along which independent gradient pulses can be applied are the x-, y-, and z-axes, represented by the unit vectors $\mathbf{i}$, $\mathbf{j}$, and $\mathbf{k}$, respectively. A pulse directed along the x-axis will produce a uniform field gradient $dB/dx = g_x(t)$ and a pulse along the y-axis will produce a uniform field gradient $dB/dy = g_y(t)$; the case for $g_z(t)$ was discussed above.

Pulsed-Field-Gradient Vectors

Pulses which are applied simultaneously along all three axes produce a combined field-gradient which is the vector sum of the three separate components:

$$\mathbf{g} = \frac{\partial B}{\partial x}\mathbf{i} + \frac{\partial B}{\partial y}\mathbf{j} + \frac{\partial B}{\partial z}\mathbf{k} = g_x(t)\mathbf{i} + g_y(t)\mathbf{j} + g_z(t)\mathbf{k}, \qquad [4]$$

where ordinary derivatives are replaced by partial derivatives because the field now varies in all three directions, i.e., $B = B(x, y, z)$. If the pulse profile $p(t)$ is the same in all three directions, we write

$$\mathbf{g} = p(t)(g_{x,m}(t)\mathbf{i} + g_{y,m}(t)\mathbf{j} + g_{z,m}(t)\mathbf{k}). \qquad [5]$$

The vector $\mathbf{g}_m$ is a constant whose magnitude $\|g_m\| = \sqrt{g_{x,m}^2(t) + g_{y,m}^2(t) + g_{z,m}^2(t)}$ is the maximum field-gradient achieved during the pulse and whose direction, represented by the unit vector $\bar{\mathbf{g}}_m = \mathbf{g}_m/\|\mathbf{g}_m\|$, is the direction of the pulse.

Generalizing Eq. [1] yields

$$R = \ln\left(\frac{S[\mathbf{g}_m]}{S[0]}\right) = -\gamma^2 P^2 \|\mathbf{g}_m\|^2 D^e, \qquad [6]$$

where the apparent diffusion coefficient in the direction of $\bar{\mathbf{g}}_m$ is defined to be

$$D^e = \bar{\mathbf{g}}_m^{\mathrm{t}}\mathbf{D}\bar{\mathbf{g}}_m, \qquad [7]$$

where the superscript t denotes the transpose of the matrix. The apparent diffusion coefficient is thus estimated from the experimental measurements by evaluating the following:

$$\Xi_i = \frac{R_i}{-\gamma^2 P^2 \|\mathbf{g}_{m,i}\|^2} = \frac{R_i}{c^2 \|\mathbf{g}_{m,i}\|^2}, \quad [8]$$

for different $\mathbf{g}_{m,i}$ values.

The Quadratic Form

On physical grounds, the diffusion tensor is expected to be symmetrical, i.e., the diffusion in any given direction is the same if the field-gradient is reversed. In this case $D_{21} = D_{12}$, $D_{31} = D_{13}$, and $D_{32} = D_{23}$. The presence of nonzero off-diagonal elements implies that there are impediments to diffusional motion that are not aligned exactly with the axes chosen for the coordinate system of the laboratory.

The apparent diffusion coefficient, after expansion of the vector–matrix–vector product in Eq. [7], is given by

$$D^e = \bar{g}_x^2 D_{11} + \bar{g}_y^2 D_{22} + \bar{g}_z^2 D_{33} + 2\bar{g}_x\bar{g}_y D_{12} + 2\bar{g}_x\bar{g}_z D_{13} + 2\bar{g}_y\bar{g}_z D_{23}. \quad [9]$$

This expression is known as the quadratic form because the components of $\bar{\mathbf{g}}_i$ occur only in products of degree two (*13*). Thus, the statistical challenge is to estimate the coefficients of this quadratic form from the experimental data Ξ_i for the various given $\bar{\mathbf{g}}_i$.

The variation in the apparent diffusion coefficient in the sample can be represented graphically by an ellipsoid, as in Fig. 1. The direction along which diffusion is measured is experimentally controlled by the appropriate choice of a combination of gradients in the three directions, to produce a gradient in the direction of $\bar{\mathbf{g}}_m$. The vector **r** in Fig. 1 is drawn in this direction; its tail is located at the origin and its point touches the inner surface of the ellipsoid. The length of **r** corresponds to the magnitude of the apparent diffusion coefficient in the direction of the vector.

Regression Analysis

Since the values of six independent elements of the diffusion tensor are to be determined, at least six different gradient directions must be used in the experiment. In addition, since each D_{ij} value was determined in the present experiments from 7, 8, or 16 different values of each of the (at least) six field gradient directions the fitting of the parameters constitutes a typical example of multivariate regression analysis (*14, 15*). Fitting the elements of the diffusion tensor (Eq. [7]) involves regression of Eq. [9] onto data quadruples that are composed of the three gradient magnitudes and the natural logarithm of the signal intensity, transformed according to the right-hand sides of Eq. [8], to give Ξ_i. The *Mathematica* function Regress performs the required analysis using the set of fitting functions $\{\bar{g}_x^2, \bar{g}_y^2, \bar{g}_z^2, 2\bar{g}_x\bar{g}_y, 2\bar{g}_x\bar{g}_z, 2\bar{g}_y\bar{g}_z\}$ that are consistent with the form of Eq. [9]. The output of the analysis includes the 3×3 diffusion tensor **D** (see Results).

Statistical bias is expected to be introduced into the estimates of the elements of **D** because of the logarithmic transformation of the original data. However, this bias can be obviated, to a large degree, by using nonlinear regression of the exponential counterpart of Eq. [1] onto the untransformed data. In the present study little difference was found between the estimates of D_{ij} and their uncertainties, obtained with either method (data not shown). Therefore, because of its greater simplicity and the ease of detecting aberrant data from Stejskal–Tanner plots, which ideally are straight lines, the linear regression approach was used thereafter.

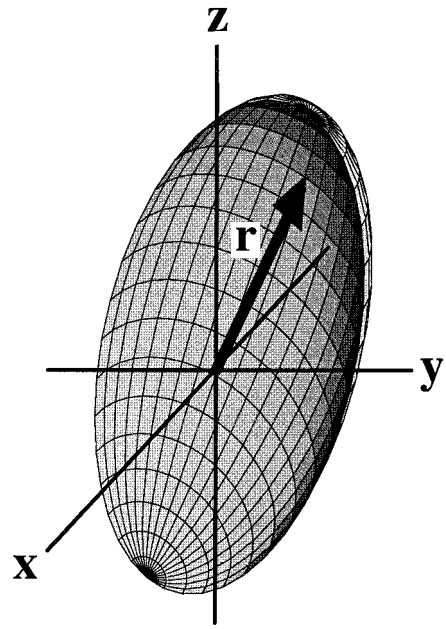

FIG. 1. Diffusion-tensor ellipsoid. The representation of diffusion anisotropy is achieved by assigning values to the three semi-axis lengths of the ellipsoid that are in the ratio of the apparent diffusion coefficients in the *x*-, *y*-, and *z*-directions in the frame of reference of the sample. The laboratory reference frame is represented as the solid lines, and the arrow denotes an arbitrary pulsed-field-gradient vector that arises from a linear combination of the basis gradient vectors $\mathbf{g}_x$, $\mathbf{g}_y$, and $\mathbf{g}_z$.

Frame Rotation

The nature of the apparent diffusion anisotropy is encapsulated in **D** which refers to a Cartesian coordinate system that has axes that are not necessarily aligned with those of the three gradient basis vectors. Therefore, the rotations that are required to bring about the transformation of the experimental frame of reference to that of the sample are achieved with the Euler rotation matrix. This matrix, **E**, rotates a Cartesian coordinate system through the angles θ, ϕ, and ψ with respect to the original *x*-, *y*-, and *z*-axes of the laboratory frame (specified by the gradient coils). Thus, the transformation of the elements of a vector **y** to give the values in the new coordinate system, **y′**, is described by

$$\mathbf{y}' = \mathbf{E}\mathbf{y}. \quad [10]$$

Because the diffusion equation (Fick's first law) specifies a linear system of vectors it has the general form

$$\mathbf{y} = \mathbf{D}\mathbf{x}, \qquad [11]$$

where **D** denotes the experimentally determined diffusion tensor.

Under the Euler transformation, Eq. [11] becomes

$$\mathbf{y}' = \mathbf{D}'\mathbf{x}', \qquad [12]$$

where $\mathbf{y}'$ is given by Eq. [10] and $\mathbf{x}' = \mathbf{E}\mathbf{x}$. Hence,

$$\mathbf{E}\mathbf{y} = \mathbf{D}'\mathbf{E}\mathbf{x}, \qquad [13a]$$

or

$$\mathbf{y} = \mathbf{E}^{-1}\mathbf{D}'\mathbf{E}\mathbf{x}. \qquad [13b]$$

Thus,

$$\mathbf{D} = \mathbf{E}^{-1}\mathbf{D}'\mathbf{E}, \qquad [14a]$$

or

$$\mathbf{D}' = \mathbf{E}\mathbf{D}\mathbf{E}^{-1}. \qquad [14b]$$

This is a similarity transform. When E is a rotation matrix, its inverse is equal to its transpose, so

$$\mathbf{D} = \mathbf{E}^{t}\mathbf{D}'\mathbf{E}, \qquad [14c]$$

or

$$\mathbf{D}' = \mathbf{E}\mathbf{D}\mathbf{E}^{t}, \qquad [14d]$$

In words, the product of the Euler matrix, that of the gradient-system diffusion tensor (determined experimentally), and the transpose of the Euler matrix, yield the diffusion tensor $\mathbf{D}'$ in the natural coordinate system of the sample. The latter tensor is a diagonal one. The coefficients of **E** are determined by the numerical diagonalization of the experimental diffusion tensor by using the *Mathematica* function SingularValues. The values of the rotation angles θ, ϕ, and ψ were obtained by using the expressions for the coefficients of the Euler matrix [using the *y*-convention of (*13*); Eq. [15]] and equating them with the corresponding elements in the experimentally determined one.

$$\mathbf{E} = \begin{bmatrix} \cos\phi\cos\theta\cos\psi - \sin\phi\sin\psi & \sin\phi\cos\theta\cos\psi - \cos\phi\sin\psi & -\sin\theta\cos\psi \\ -\cos\phi\cos\theta\sin\psi - \sin\phi\cos\psi & -\sin\phi\cos\theta\sin\psi + \cos\phi\cos\psi & \sin\theta\sin\psi \\ \sin\theta\cos\phi & \sin\theta\sin\phi & \cos\theta \end{bmatrix}. \qquad [15]$$

The natural coordinate system thus formed is the set of principal axes of the ellipsoid and the three elements of the diagonal of $\mathbf{D}'$ are the lengths of the semi-axes in the direction of the three principal axes, such as that drawn in Fig. 1.

EXPERIMENTAL

Erythrocytes. Blood was obtained by venipuncture from the median-cubital vein of the donor (PWK). The cells were washed twice by centrifugation (3000*g* at 4°C) in 4 vol of physiological saline (NaCl, 0.9% w/v) containing 10 mM glucose. After the second wash the cell suspension was gassed with CO to convert the hemoglobin to the diamagnetically stable form that is optimal for NMR studies of these cells [e.g., (*1*)]. To swell the cells, some of the cell pellet was suspended in 4 vol of 121 mM NaCL containing 10 mM glucose, while to shrink the cells, to be more like a flat disc, they were suspended in 242 mM NaCl also containing 10 mM glucose. The suspended cells were then sedimented by centrifugation as before. All cell samples were suspended to give a final hematocrit of ~0.65; this value was chosen because it provided a relatively large extracellular space without allowing significant settling of the cells during the time of the experiment.

NMR samples. A total of 0.5 mL of the erythrocyte suspension was placed in 5-mm-od glass NMR tubes (507-PP, Wilmad, Buena, NJ).

NMR spectrometer. The experiments were conducted on a Bruker DRX-400 spectrometer (Karlsruhe, Germany) with an Oxford Instruments 9.4-T vertical wide-bore magnet (Oxford, UK) with a Bruker TXI 5-mm, ~500 mT m^{-1} *x*-, *y*-, and *z*-axis gradient probe. The sample temperature was controlled at 298 K. PGSE experiments were conducted as described previously (*1–3*). The pulse-sequence parameters were: duration of field-gradient pulses, $\delta = 2$ ms; time interval between field-gradient pulses, $\Delta = 20$ ms; 90° RF pulse, 12–13 μs; total spin-echo time, TE = 40 ms; 8 transients per spectrum; maximum field-gradient, $g_{r,\max} = 0.5$ T m^{-1}. Routinely 16 spectra were

acquired with a sequential increase in the value of g. The three gradients were calibrated using the known diffusion coefficient of water in an isotropic and unbounded space (*16*).

Data analysis. In each spectrum, the integral of the water resonance was measured using the standard Bruker software (*uxnmr*) where it was normalized with respect to the signal intensity in the first spectrum. Unless the first spectrum was acquired with a small nonzero gradient its phase was substantially different from that of the rest in the series. Therefore, a value of 1 G cm^{-1} was used for the field-gradient magnitude in the first spectrum of each series. The subsequent analysis in a *Mathematica* program followed that described under Theory and in the Appendix.

RESULTS

Erythrocytes in Isotonic Medium

Figure 2A shows a set of ^{1}H PGSE NMR signal intensities obtained from the water in normal-volume human erythrocytes and their extracellular medium. The sample was subjected to a range of values of the following gradients: $\mathbf{g}_x$, $\mathbf{g}_y$, $\mathbf{g}_z$, $\mathbf{g}_{xy}$, $\mathbf{g}_{xz}$, $\mathbf{g}_{yz}$, and $\mathbf{g}_{xyz}$. The composite gradients such as $\mathbf{g}_{xy}$ were generated from the appropriate combination of the basis gradients. The latter were adjusted so that the resultant gradient had the same magnitude as those used in experiments where the basis gradients were applied singly. Fine adjustments to scaling factors for the gradient magnitudes were made during data analysis; these were based on the measurement of the apparent diffusion coefficient of water in all directions and the assumption that it should have the same value in all directions (*16*).

The bottom 16 points (▼) in Fig. 2A were obtained with the field-gradient applied along the z-direction (direction of $\mathbf{B}_0$). The upper set was obtained with the gradient in the x-direction (◆), and these were superimposed upon by those acquired with the field gradient in the y-direction and in the x,y-direction (◇). The next most rapid signal attenuation was obtained with the $\mathbf{g}_{xz}$- and $\mathbf{g}_{yz}$-data. Hence, diffusion in the direction of $\mathbf{g}_z$ was significantly more rapid than in all other directions.

It is also readily seen in Fig. 2A that each data set was not well described by a single straight line. However, a straight line fitted each data set moderately well over the first eight points of each set and even better for the second to the eighth points; the outcome of fitting this truncated sets of the points is shown in Fig. 2B. The four straight lines had significantly different (t test) slopes in the order $\mathbf{g}_z$-data > superimposed $\mathbf{g}_{xz}$–$\mathbf{g}_{yz}$-data > $\mathbf{g}_{xyz}$-data > superimposed $\mathbf{g}_x$–$\mathbf{g}_y$–$\mathbf{g}_{xy}$-data. The slopes of the latter three lines were not significantly different and the symbols used for the g_x- and g_y-data in Fig. 2B were superimposed.

Erythrocytes in Hyper- and Hypotonic Media

Experiments, the same as those used for Fig. 2, were carried out on cells that were flattened by the osmotic effect of a hypertonic saline solution (*2, 17*). The qualitative features of the Stejskal–Tanner plots were the same as in Fig. 2A but the extent of signal attenuation was greater for each of the seven different field-gradient directions (Fig. 3). This effect was quantified when the data were fitted by straight lines to the 2nd to the 8th or the 9th to the 16th points in each set.

When human erythrocytes are placed in hypotonic saline they take on an almost spherical shape while retaining two diametrically opposed indentations (*2, 17*). Not withstanding the more spherical shape of the cells, the two regression lines still revealed a greater apparent diffusion coefficient for the z-direction compared with all others. To avoid overcrowding

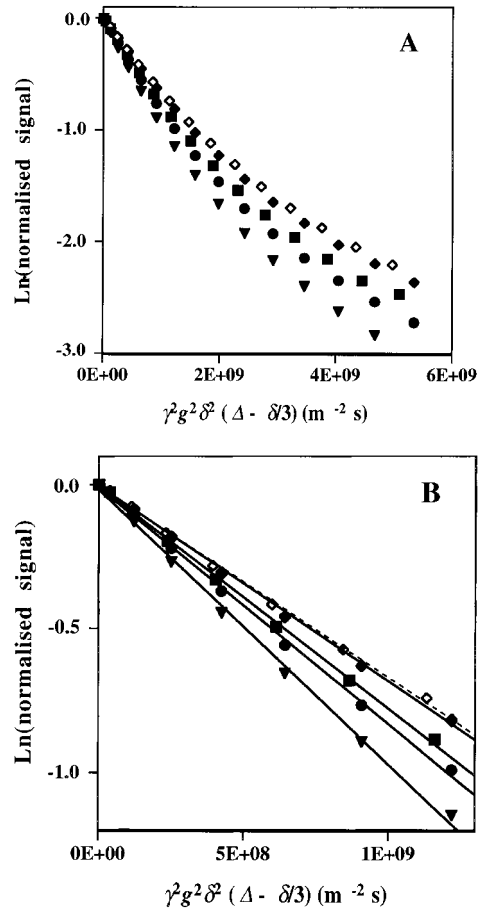

FIG. 2. Signal intensity from water, as a function of the magnitude and direction of the magnetic field-gradient pulses in ^{1}H NMR PGSE experiments conducted on a suspension of normal-volume human erythrocytes, at a hematocrit of 0.65 and temperature of 25°C. The graphs are in the format proposed by Stejskal and Tanner (*12*) and the independent (abscissal) variable is accordingly referred to as the Stejskal–Tanner parameter. Seven data sets were acquired for each of 16 different values of the gradient pulses. A. The gradients and their corresponding data sets are denoted by the symbols: $\mathbf{g}_x$, ◆; $\mathbf{g}_y$, ◆; $\mathbf{g}_z$, ▼; $\mathbf{g}_{xy}$, ◇; $\mathbf{g}_{xz}$, ●; $\mathbf{g}_{yz}$, ●; $\mathbf{g}_{xyz}$, ■. Note that the data for $\mathbf{g}_x$ were superimposed on those of $\mathbf{g}_y$, and similarly for $\mathbf{g}_{xz}$ and $\mathbf{g}_{yz}$. B. A replot of the data in A, but taking only the first eight points and fitting those with a straight line: the symbols are as for A. Each fitted line is clearly associated with a particular data set.

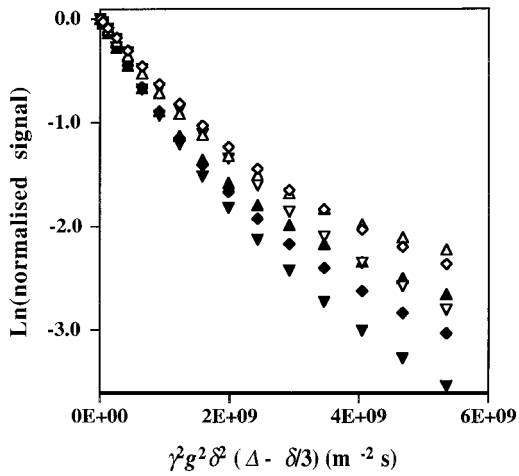

FIG. 3. Stejskal–Tanner plot of the ^{1}H NMR PGSE signal intensity obtained from human erythrocytes of three different average volumes and with the pulsed-field-gradients applied in the *x*- and *z*-directions only, for a range of 16 different values. The average volume of the cells, the gradient, and the symbols used were as follows: swollen cells, $\mathbf{g}_x$, △; swollen cells, $\mathbf{g}_z$, ▲; normal-volume cells, $\mathbf{g}_x$, ◇; normal-volume cells, $\mathbf{g}_z$, ◆; shrunken (flattened) cells, $\mathbf{g}_x$, ▽; shrunken cells, $\mathbf{g}_z$, ▼.

the graph, the data for only the *x*- and *z*-directions were presented in Fig. 3.

Diffusion Tensor

The data in Fig. 2A, and the corresponding sets for erythrocytes suspended in hypotonic and hypertonic media, were subjected to quantitative diffusion tensor analysis. This was carried out according to the procedure described under Experimental by using the program presented in the Appendix. Table 1 contains the results of the analysis of the second to eighth points in each Stejskal–Tanner plot; it confirmed in a quantitative way the impression gained from Fig. 2A regarding less restriction of diffusion in the *z*-direction than all others. For the normal-volume cells the values of D_{11} and D_{22} (average, 6.98×10^{-10} m^2 s^{-1}) were the same within the experimental error and the coefficient of variation was ~2.5%. The error was substantially greater (coefficient of variation ~17%) when the first point was included in the regression, hence its blanking out in all subsequent analyses (see Discussion). The coefficients of variation for the estimates of the three leading-diagonal terms were less for the first half of a data set than for the second half; this is consistent with the appearance of a greater degree of curvature of the plots (Figs. 2A and 3) for larger vales of the Stejskal–Tanner parameter.

In Table 1 the estimate of D_{33} was $10.20 \pm 1.00 \times 10^{-10}$ m^2 s^{-1}, which was more than two standard deviations different from the corresponding D_{11} and D_{22} values. The other elements of the diffusion tensor (the cross-terms) were not significantly different from zero.

For the second to eighth data points in each set, the normal-volume erythrocytes had a difference between the average of their values of D_{11} and D_{22} and the value of D_{33} of 3.25×10^{-10} m^2 s^{-1}; but for the swollen and flattened cells it was 2.53×10^{-10} and 3.14×10^{-10} m^2 s^{-1}, respectively. The largest difference was with the normal-volume cells. On the other hand, when the last eight point were analyzed (Table 2) the corresponding differences were substantially less, while the largest difference was with the flattened cells. The differences were 1.7×10^{-10}, 1.2×10^{-10}, and 1.9×10^{-10} m^2 s^{-1}, respectively.

Furthermore, Fig. 3 provides graphical representation of the fact that the apparent diffusion coefficient in the *x*- and *z*-directions was greatest for the cells in the hypertonic medium, followed by the normovolumic cells, and then the swollen cells.

TABLE 1

Results of the Multivariate Linear Regression Analysis of PGSE ^{1}H NMR Data from Human Erythrocytes That Were Suspended in Isotonic (154 mM), Hypotonic (121 mM), and Hypertonic (242 mM) Saline Solutions

	Parameter ($10^{10} \times$ m^2 s^{-1})	Estimate ($10^{10} \times$ m^2 s^{-1})	SE ($10^{10} \times$ m^2 s^{-1})	Sample frame
Isotonic	x^2 (D_{11})	6.88	0.17	6.80
	y^2 (D_{22})	7.07	0.17	7.16
	z^2 (D_{33})	10.20	0.17	10.20
	$2xy$ (D_{12})	−0.31	0.19	
	$2xz$ (D_{13})	0.16	0.19	
	$2yz$ (D_{23})	0.0009	0.19	
Hypotonic	x^2 (D_{11})	7.99	0.23	8.01
	y^2 (D_{22})	7.50	0.23	7.47
	z^2 (D_{33})	10.27	0.23	10.27
	$2xy$ (D_{12})	−0.20	0.26	
	$2xz$ (D_{13})	0.17	0.25	
	$2yz$ (D_{23})	0.24	0.25	
Hypertonic	x^2 (D_{11})	7.35	0.12	7.43
	y^2 (D_{22})	7.21	0.12	7.11
	z^2 (D_{33})	10.42	0.12	10.43
	$2xy$ (D_{12})	0.30	0.26	
	$2xz$ (D_{13})	0.21	0.26	
	$2yz$ (D_{23})	0.38	0.26	

Note. The 2nd to the 8th points from a total of 16 were used in the analysis; this corresponded to the first linear section of the data set (see Fig. 2B). (It was repeatedly noted, and also in the present data set, that avoidance of using the 1st point in the analysis reduced the coefficient of variation (SE) in the D_{ii} estimates from ~17 to ~3%, hence its omission here.) The basis functions used in the regression of the quadratic form (Eq. [9]) onto the data are those listed in the first column together with the corresponding element of the diffusion tensor (Eq. [3]). The second column contains the estimates of the values of the elements; most notable are the first three values that correspond to the diffusion coefficients in the *x*-, *y*-, and *z*-directions. The SE column contains the standard errors of the parameter estimates that is a standard output of the *Mathematica* function (see Appendix). The right-hand column contains the elements of the diagonalized matrix and these values correspond to the diffusion coefficients in the *x*-, *y*-, and *z*-directions, respectively, in the frame of reference of the sample.

TABLE 2
Results of the Multivariate Linear Regression Analysis of the Second Set of Eight Points in Each Data Set

	Parameter ($10^{10} \times m^2\ s^{-1}$)	Estimate ($10^{10} \times m^2\ s^{-1}$)	SE ($10^{10} \times m^2\ s^{-1}$)	Sample frame
Isotonic	x^2 (D_{11})	5.62	0.30	5.66
	y^2 (D_{22})	5.46	0.30	5.41
	z^2 (D_{33})	7.27	0.30	7.72
	$2xy$ (D_{12})	−0.18	0.33	
	$2xz$ (D_{13})	0.13	0.33	
	$2yz$ (D_{23})	0.16	0.33	
Hypotonic	x^2 (D_{11})	5.60	0.38	5.59
	y^2 (D_{22})	5.30	0.38	5.29
	z^2 (D_{33})	6.69	0.38	6.70
	$2xy$ (D_{12})	−0.19	0.42	
	$2xz$ (D_{13})	0.17	0.42	
	$2yz$ (D_{23})	0.20	0.42	
Hypertonic	x^2 (D_{11})	6.22	0.27	6.19
	y^2 (D_{22})	6.30	0.27	6.29
	z^2 (D_{33})	8.14	0.27	8.17
	$2xy$ (D_{12})	−0.04	0.60	
	$2xz$ (D_{13})	0.28	0.59	
	$2yz$ (D_{23})	0.37	0.59	

Note. The meaning of each column in the table is the same as for Table 1.

DISCUSSION

Two Major Diffusion Domains

The experimental data in Figs. 2 and 3 showed that diffusion of water was less restricted in the z-direction than in all others. The superposition of the $\mathbf{g}_x$–$\mathbf{g}_y$–$\mathbf{g}_{xy}$-data showed that there was no preferred ordering of the cells when projected onto the x,y-plane.

The diagonal element of **D** (Tables 1 and 2) with the largest value, D_{33}, corresponding to the apparent diffusion coefficient for water that was both inside and outside the cells in the suspension of normal-volume erythrocytes in the z-direction, was $(10.2 \pm 1.00) \times 10^{-10}\ m^2\ s^{-1}$; but this value is substantially less than $\sim 2 \times 10^{-9}\ m^2\ s^{-1}$ expected for water in an isotropic unbounded saline solution (*16*). This is clear evidence that the diffusion of water was impeded in the erythrocyte suspensions. Furthermore, the general nonconformity of the data sets shown in Fig. 2A with straight lines implies that the water was undergoing restricted and/or obstructed diffusion in at least two spatial domains. This is consistent with the water in the cell suspensions occupying both the intra- and extracellular spaces. Because water exchanges rapidly across the cell membranes there is a blurring of the effects of restriction of motion in one compartment by that in the other. The water outside the cells moved with a larger apparent diffusion coefficient than that inside, which was restricted by the cell membranes (*1*). Nevertheless, the extracellular diffusion is obstructed by the outside of the cell membranes and so the apparent diffusion coefficient is dependent on the packing density (hematocrit) of the suspension; as such it is a parameter that is readily under experimental control.

Correlation with Cell Diameter

The NMR signal that persisted at the higher values of the field-gradient would have been that from water that had the smallest apparent diffusion coefficient, namely water inside the cells. The second to eighth points, and the last eight points, of each data set were moderately well described by separate straight lines but the regression-fit was better for the first set. It is worth emphasizing that the subdivision of the points was arbitrary and was based simply on separating the data into the first and last half of each set.

From previous q-space analysis of erythrocyte suspensions (*1–3*) it is known that for larger values of the field gradients the signal that remains is primarily from the water inside the cells. In the previous q-space analysis of red cell suspensions the conclusion regarding alignment of the cells with their disc planes parallel to $\mathbf{B}_0$ was based on the consistency of the position of the first diffusion–diffraction minimum with a scalar distance that was equal to the known main diameter of the human red cell (*18*).

The area of the membrane of a human erythrocyte does not change significantly as it shrinks or swells (*19*); an increase in the volume only comes about by the biconcave disc becoming more spherical and hence taking a smaller main diameter. Therefore, the values of D_{33} for the cells of different sizes should be reflected in the relative magnitude of this parameter. Indeed, this was the case (see Table 2), with D_{33} being $(6.69 \pm 0.38) \times 10^{-10}\ m^2\ s^{-1}$ for the swollen cells with the smallest main diameter, $(7.27 \pm 0.30) \times 10^{-10}\ m^2\ s^{-1}$ for cells of normal volume, and $(8.14 \pm 0.27) \times 10^{-10}\ m^2\ s^{-1}$ for the cells that were flattened and therefore had the largest diameter.

Euler Angles

The fifth columns of Tables 1 and 2 show that after diagonalizing the experimentally determined **D** there was no statistically significant change in the values of the diagonal elements of the tensor. This implies that the sample frame of reference was aligned with that defined by the magnetic field-gradients.

The Appendix shows one example of a set of angles ($\theta = 91°$, $\phi = 30°$, and $\psi = 1°$) that were required to align the laboratory (gradient) frame of reference with the sample frame. This set relates to the second to eighth points from the isotonic sample referred to in Table 1. The *Mathematica* function SingularValues diagonalizes a matrix and then places the elements of the diagonal matrix in echelon form, from left to right down the leading diagonal. Thus the element D_{33} in the experimental tensor was moved to the position of D_{11} in the diagonal matrix. Since the original experimental tensor was almost diagonal the value of θ would be expected to be near 90°, as was the case. The fact that ϕ was not 0° or 90° was also evident with the other analyses, and this is consistent with the high

level of statistical noise in the off-diagonal terms of the experimental tensor. In other words, the similarity of the values of the elements on the leading diagonal in the experimental tensor with those of its diagonalized form (Tables 1 and 2) showed that, within experimental error, the cells were aligned with their disc planes parallel to the direction of $\mathbf{g}_z$ and $\mathbf{B}_0$.

Statistics

A final comment on the statistical analysis is warranted. The output from the *Mathematica* program (see Appendix) contains valuable information in addition to the values of the elements of the diffusion tensor. These items include the standard errors (SE) of the parameter estimates, *t* statistic, and *P* value. The latter were minute ($\ll 0.01$) in all cases for the diagonal elements, indicating a high level of statistical significance of the estimated values and their consistency with the fitted quadratic form (Eq. [9]). A large change was noticed in the SEs estimated in the regression analysis of the first eight points, when the first point in each set was eliminated. This effect was traced to the fact that the first spectrum, acquired with a low value of field-gradient, was usually not of consistent intensity compared with the others in the series. Since the points lay at the extremes (beginning) of the series of fitted points it was deemed justified to eliminate them from the analysis.

Conclusions

The clinical significance of the alignment of erythrocytes in a magnetic field, as demonstrated here, is unknown as the cells were not flowing. The effect of flow on the alignment of erythrocytes *in vivo* is imperfectly understood; but it is conceivable that the microperfusion of tissues could be altered as a result of the different orientations of the perfusing blood vessels and the alignment of the erythrocytes in them (*1*). Since red cells become distorted when passing through capillaries, such effects would presumably only be manifest in the larger arterioles and venules that feed and drain the capillary beds, respectively.

The physical basis of the alignment of the discocytes in $\mathbf{B}_0$ is primarily the diamagnetic anisotropy of the phospholipids in the membranes, with some opposing contribution from the differences between the bulk magnetic susceptibility across the cell membrane (*3*, *20*).

A systematic approach to estimating the diffusion tensor from PGSE data was developed using functions available in *Mathematica*. This provided a compact and rapid analytical strategy for evaluating the Euler rotation matrix and defining the relationship between the laboratory and sample Cartesian-reference frames. While quantitative determinations of the values of the elements of the diffusion tensor are generally not sought in MRI, these values are required for a precise description of the rate of solvent and solute diffusion in biophysical studies of tissues and cells. Thus a suspension of carbonmonoxygenated human erythrocytes may serve as a well-characterized diffusion-tensor phantom for calibrating an MRI instrument for quantitative biophysical studies.

APPENDIX

The *Mathematica* program was used with PGSE NMR data to calculate: (1) the diffusion tensor in the laboratory frame of reference; (2) the diagonalized form of the tensor and hence the tensor in the frame of reference of the sample; and (3) the Euler rotation matrix that specifies the frame of reference of the sample relative to the laboratory frame. The Input commands are given in boldface and the Input comments and Output statements are in plain text. The input and output values/numbers are from the actual experiment whose data are given in Fig. 2. The fit was to the 2nd to the 8th points in each set of 16 4-tuples. The blanking off of the primary data was done with the bracket–asterisk comment declarer.

```
(*Diffusion tensor calculation from PGSE data*)
In[1]:=
Needs["Statistics`LinearRegression`"]
gam = 2.67 × 10^8; (*γ radians s^-1, magnetogyric ratio of protons*)
lildel = 0.002; (*δ seconds, duration of field-gradient pulse*)
bigdel = 0.02; (*Δ seconds, time interval between field-gradient pulses*)
stejTan = gam^2 lildel^2 (bigdel − lildel/3); (*Stejskal–Tanner variable*)

(*data consist of the 4-tuples {gx, gy, gz, signal} where the signal has been normalized, in uxnmr, with respect to that in the
first spectrum for which the gradient has the least value*)
data =
{(*{0.01, 0.0, 0.0, 1.0},*)(*1st 4-tuple, first gx value, gy, gz = 0; signal = 1.0*)
                            (*blanking off the 1st 4-tuple improves quality of fit*)
{0.043, 0.0, 0.0, 0.9780},
```

```
                •
                • (*blanking off the 9th to the 16th 4-tuple to fit first linear section*)
                •
{0.5, 0.0, 0.0, 0.09408},*) (*16th 4-tuple, last gx value, gy, gz = 0*)

(*{0.0, 0.01, 0.0, 1.0},*)(*1st 4-tuple, first gy value, gx, gz = 0; signal = 1.0*)
                          (*blanking off the 1st 4-tuple improves quality of fit*)
  {0.0, 0.043, 0.0, 0.9749},
                •
                •(*blanking off the 9th to the 16th 4-tuple to fit first linear section*)
                •
  {0.0, 0.5.0, 0.0, 0.09605), *) (*16th 4-tuple, last gy value, gx, gz = 0*)
                •
                •
                •     (*16 × 4-tuples, only gz applied*)
                •     (*16 × 4-tuples, gx and gy applied*)
                •     (*16 × 4-tuples, gx and gz applied*)
                •     (*16 × 4-tuples, gy and gz applied*)
                •     (*16 × 4-tuples, gx, gy, and gz applied*)
                  };
```

(*transform the data so that the 4th element in the 4-tuple is divided by the Stejskal–Tanner parameter that includes the maximum gradient squared (according to Eq. [8] in the text), and the field-gradient elements are normalized by dividing by the length of the gradient vector, namely the square root of the sum of the squares of the magnitudes of the three constituent basis gradients*)

```
trans[x_,y_]:= −Log[x]/(stejTan*y^2)
transdat = Partition[Flatten[Map[{{Part[#,1],Part[#,2],Part[#,3]}/
  (Sqrt[Part[#,1]^2+Part[#,2]^2+Part[#,3]^2),trans[Part[#,4],
  Sqrt[Part[#,1]^2+Part[#,2]^2+Part[#,3]^2] ]}&,data]], 4];
```

(*the quadratic form of Eq. [9], described by the gradient basis functions, is fitted onto the data*)

```
fitr = Resgress[transdata, {x^2, y^2, z^2, 2 x y, 2 x z, 2 y z}, {x, y, z},
                    IncludeConstant→False]
```

Out[2]=
{ParameterTable→

	Estimate	SE	TStat	PValue
x^2	6.89×10^{-10}	1.72×10^{-11}	40.0093	0.
y^2	7.07×10^{-10}	1.72×10^{-11}	41.0547	0.
z^2	1.02×10^{-9}	1.72×10^{-11}	59.4686	0. ,
$2\ x\ y$	-3.12×10^{-11}	1.87×10^{-10}	−1.65917	0.104358
$2\ x\ z$	1.59×10^{-11}	1.86×10^{-10}	0.858712	0.395261
$2\ y\ z$	-8.82×10^{-11}	1.86×10^{-10}	−0.0047507	0.996231

RSquared → 0.982403, AdjustedRSquared → 0.980291,
EstimatedVariance → 7.68077×10^{-21}, ANOVATable →

	DF	SumOfSq	MeanSq	FRatio	PValue
Model	6	3.24×10^{-17}	5.39×10^{-18}	2498.09	0.
Error	43	9.28×10^{-20}	2.16×10^{-21}		}
U Total	49	3.25×10^{-17}			

(*repeat fit and extract diffusion tensor from Output Table*)
In[3]=

```
fitr = Regress[transdata, {x^2, y^2, z^2, 2 x y, 2 x z, 2 y z}, {x, y, z},
       IncludeConstant→False, RegressionReport →
       {ParameterConfidenceRegion}];
resf = ParameterConfidenceRegion/.fitr[[1]];
dt = resf[[1]];

diffTens = {{dt[[1]], 0.5 dt[[4]], 0.5 dt[[5]]},
            {0.5 dt[[4]], dt[[2]], 0.5 dt[[6]]},
            {0.5 dt[[5]], 0.5 dt[[6]], dt[[3]]}};
{u, md, v} = SingularValues[diffTens]
MatrixForm[DiagonalMatrix[md]]
```

Out[4]=

$$\{\{\{0.024, -0.0013, 0.100\}, \{-0.498, 0.867, 0.013\}, \{0.867, 0.498, -0.020\}\}, \{1.02 \times 10^{-9}, 7.16 \times 10^{-10}, 6.79 \times 10^{-10}\}, \{0.024, -0.0013, 0.100\}, \{-0.498, 0.867, 0.013\}, \{0.867, 0.498, -0.020\}\}\}$$

Out[5]=

$$\begin{bmatrix} 1.02041 \times 10^{-9} & 0 & 0 \\ 0 & 7.15563 \times 10^{-10} & 0 \\ 0 & 0 & 6.79495 \times 10^{-10} \end{bmatrix}$$

In[6]=

```
(*the Euler matrix is as follows:
rotMat:={{Cos[fi]Cos[th]Cos[psi]-Sin[fi]Sin[psi],Sin[fi]Cos[th]Cos[psi]+
Cos[fi]Sin[psi],-Sin[th]Cos[psi]},{-Cos[fi]Cos[th]Sin[psi]-
Sin[fi]Cos[psi],-Sin[fi]Cos[th]Sin[psi]+Cos[fi]Cos[psi],
Sin[th]Sin[psi]},{Sin[th]Cos[fi],Sin[th]Sin[fi],Cos[th]}}.
To determine fi, theta, and psi, equate elements (3,3), (3,2), and (2,3)
with the corresponding terms of the Euler matrix and solve for each angle*)
```

In[7]=

```
theta = ArcCos[ut[[3,3]]]*180/Pi//N
phi = ArcSin[ut[[3,2]]/Sin[ArcCos[ ut[[3,3]] ] ]*180/Pi//N
psi = ArcSin[ut[[2,3]]/Sin[ArcCos[ ut[[3,3]] ] ]*180/Pi//N
```

Out[8]= 91.1586

Out[9]= 29.8692

Out[10]= 0.753636

ACKNOWLEDGMENTS

This work was part of a project that was funded by the Australian Research Council. We thank Dr. Bill Bubb for valuable contributions to the NMR spectrometer and spectroscopy, Mr. Bill Lowe for expert technical assistance, and Dr. Peter Mulquiney for pointing out the linear regression function of *Mathematica*. P.S.J. was a visiting elective student from St. Bartholomew's and the Royal London Medical School.

REFERENCES

1. P. W. Kuchel, A. Coy, and P. Stilbs, NMR "diffusion–diffraction" of water revealing alignment of erythrocytes in a magnetic field and their dimensions and membrane transport characteristics, *Magn. Reson. Med.* **37,** 637–643 (1997).
2. A. M. Torres, R. J. Michniewicz, B. E. Chapman, G. A. R. Young, and P. W. Kuchel, Characterisation of erythrocyte shapes and sizes by NMR diffusion–diffraction of water: Correlation with electron micrographs, *Magn. Reson. Imaging* **16,** 423–434 (1998).
3. A. M. Torres, A. T. Taurins, D. G. Regan, B. E. Chapman, and P. W. Kuchel, Assignment of coherence features in NMR q-space plots to particular diffusion modes in erythrocyte suspensions, *J. Magn. Reson.* **138,** 135–143 (1999).
4. P. J. Basser, J. Mattiello, and D. LeBihan, Estimation of the effective self-diffusion tensor from the NMR spin echo. *J. Magn. Reson. B* **103,** 247–254 (1994).

5. P. J. Basser and C. Pierpaoli, Microstructural and physiological features of tissues elucidated by quantitative-diffusion-tensor MRI. *J. Magn. Reson. B* **111,** 209–219 (1996).
6. A. M. Ulug and P. C. M. van Zijl, Orientation-independent diffusion imaging without tensor diagonalisation: Anisotropy definitions based on physical attributes of the diffusion ellipsoid. *J. Magn. Reson. Imaging* **9,** 804–813 (1999).
7. W-Y. I. Tseng, T. G. Reese, R. M. Weisskoff, and V. J. Weeden, Cardiac diffusion tensor MRI without in vivo strain correction. *Magn. Reson. Med.* **42,** 393–403 (1999).
8. D. K. Jones, M. A. Horsfield, and A. Simmons, Optimal strategies for measuring diffusion in anisotropic systems by magnetic resonance imaging. *Magn. Reson. Med.* **42,** 515–525 (1999).
9. S. Pajevic and C. Pierpaoli, Color schemes to represent the orientation of anisotropic tissues from diffusion tensor data: Application to white matter fiber tract mapping in the human brain. *Magn. Reson. Med.* **42,** 526–540 (1999).
10. P. van Gelderen, D. DesPres, P. C. M. van Zijl, and C. T. Moonen, Evaluation of restricted diffusion in cylinders. Phosphocreatine in rabbit leg muscle, *J. Magn. Reson. B* **103,** 255–260 (1994).
11. S. Wolfram, "The Mathematica Book," Cambridge Univ. Press, Cambridge (1999).
12. E. O. Stejskal and J. E. Tanner, Spin diffusion measurements: Spin-echoes in the presence of a time-dependent field gradient. *J. Chem. Phys.* **42,** 288–292 (1965).
13. H. Goldstein, "Classical Mechanics," Second ed., Addison–Wesley, Reading (1980).
14. B. T. Bulliman, P. W. Kuchel, and B. E. Chapman, "Overdetermined" one dimensional NMR exchange analysis: A 1-D counterpart of the 2-D EXSY experiment. *J. Magn. Reson.* **82,** 377–384 (1989).
15. M. L. Abell, J. P. Braselton, and J. A. Rafter, "Statistics with Mathematica," Version 3, Academic Press, San Diego (1999).
16. R. Mills, Self-diffusion in normal and heavy water in the range 1–45°. *J. Phys. Chem.* **77,** 685–688 (1973).
17. Z. H. Endre, B. E. Chapman, and P. W. Kuchel, Cell volume dependence of ^{1}H spin echo NMR signals in human erythrocyte suspensions: The influence of in situ field gradients. *Biochim. Biophys. Acta* **803,** 137–144 (1984).
18. J. V. Dacie and S. M. Lewis, "Practical Haematology," Churchill Livingstone, Edinburgh (1975).
19. A. J. Grimes, "Human Red Cell Metabolism," Blackwell Sci., Oxford (1980).
20. T. Higashi, A. Yamagishi, T. Takeuchi, N. Kawaguchi, S. Sagawa, S. Onishi, and M. Date, Orientation of erythrocytes in a strong magnetic field. *Blood* **82,** 1328–1334 (1993).